Cancer Research

Membrane-Depolarizing Channel Blockers Induce Selective Glioma Cell Death by Impairing Nutrient Transport and Unfolded Protein/Amino Acid Responses

Mia Niklasson[1,2], Gianluca Maddalo[3], Zuzana Sramkova[2,4], Ercan Mutlu[5], Shimei Wee[2], Petra Sekyrova[2,4], Linnéa Schmidt[1], Nicolas Fritz[6], Ivar Dehnisch[7], Gregorios Kyriatzis[2], Michaela Krafcikova[4], Brittany B. Carson[2,8], Jennifer M. Feenstra[2,8], Voichita D. Marinescu[1], Anna Segerman[1], Martin Haraldsson[9], Anna-Lena Gustavsson[9], Lars G.J. Hammarström[9], Annika Jenmalm Jensen[9], Lene Uhrbom[1], A.F. Maarten Altelaar[3], Sten Linnarsson[7], Per Uhlén[7], Lukas Trantirek[4], C. Theresa Vincent[2,8], Sven Nelander[1], Per Øyvind Enger[5,10], and Michael Andäng[2,4]

Abstract

Glioma-initiating cells (GIC) are considered the underlying cause of recurrences of aggressive glioblastomas, replenishing the tumor population and undermining the efficacy of conventional chemotherapy. Here we report the discovery that inhibiting T-type voltage-gated Ca^{2+} and K_{Ca} channels can effectively induce selective cell death of GIC and increase host survival in an orthotopic mouse model of human glioma. At present, the precise cellular pathways affected by the drugs affecting these channels are unknown. However, using cell-based assays and integrated proteomics, phosphoproteomics, and transcriptomics analyses, we identified the downstream signaling events these drugs affect. Changes in plasma membrane depolarization and elevated intracellular Na^+, which compromised Na^+-dependent nutrient transport, were documented. Deficits in nutrient deficit acted in turn to trigger the unfolded protein response and the amino acid response, leading ultimately to nutrient starvation and GIC cell death. Our results suggest new therapeutic targets to attack aggressive gliomas. *Cancer Res; 77(7); 1741–52. ©2017 AACR.*

Introduction

Glioblastoma multiforme (GBM) is a highly heterogeneous brain tumor with a population of cancer cells endowed with glioma tumor-initiating capacity, the glioma-initiating cells (GIC; refs. 1, 2). These cells share gene expression with stem cells (3, 4) and continuously resupply the bulk tumor through self-renewal and differentiation (5). GICs have high drug efflux capacity and slow proliferation rate, which results in increased chemo- and radiotherapy resistance (6, 7), fostering rapid tumor relapse after therapy. Hence, there is an urgent need for therapies that would specifically target this tumor cell population, sparing normal cells. In line with other researchers (8, 9), we recently showed that tumor-initiating cells are sensitive to disturbed Ca^{2+} homeostasis (10), making ion channels appealing targets in GICs. Noteworthy, ion channels are also known to be dysregulated during cancer formation and progression (11).

The human genome encodes approximately 400 ion channels, which control a multitude of biological processes such as ion and osmotic homeostasis and nutrient import, all vital for cell viability. For example, voltage-gated calcium channels (VGCC) trigger catabolic cellular responses in cancer cells (12, 13). However, the causal signaling pathways preceding this phenomenon are unknown, although stimulation of nonselective transient receptor potential cation channels (TRPV1) in GICs has been shown to compromise their viability via endoplasmic reticulum (ER) stress (14).

Here, we screened a library of ion channel blockers in 44 different GICs and identified sets of ion channel blockers that selectively impaired viability of GICs, and increased survival in a mouse model of human GBM. Importantly, using a systems

[1]Department of Immunology, Genetics and Pathology, Science for Life Laboratory, Uppsala University, Uppsala, Sweden. [2]Department of Physiology and Pharmacology, Karolinska Institutet, Stockholm, Sweden. [3]Biomolecular Mass Spectrometry and Proteomics, Bijvoet Center for Biomolecular Research and Utrecht Institute for Pharmaceutical Science, Utrecht University, Utrecht, the Netherlands. [4]Central European Institute of Technology, Masaryk University, Brno, Czech Republic. [5]Oncomatrix Research Lab, Department of Biomedicine, University of Bergen, Bergen, Norway. [6]Science for Life Laboratory, Department of Applied Physics, Royal Institute of Technology, Stockholm, Sweden. [7]Department of Medical Biochemistry and Biophysics, Karolinska Institutet, Stockholm, Sweden. [8]Department of Physiology and Biophysics, Weill Cornell Medical College, New York, New York. [9]Chemical Biology Consortium Sweden, Division of Translational Medicine and Chemical Biology, Department of Medical Chemistry and Biophysics, Karolinska Institutet, Stockholm, Sweden. [10]Department of Neurosurgery, Haukeland University Hospital, Bergen, Norway.

Note: Supplementary data for this article are available at Cancer Research Online (http://cancerres.aacrjournals.org/).

M. Niklasson, G. Maddalo, Z. Sramkova, E. Mutlu, and S. Wee contributed equally to this article.

Corresponding Author: Michael Andäng, Department of Physiology and Pharmacology, Karolinska Institutet, Stockholm 171 77, Sweden. Phone: 46-0-703-314682; E-mail: michael.andang@ki.se

doi: 10.1158/0008-5472.CAN-16-2274

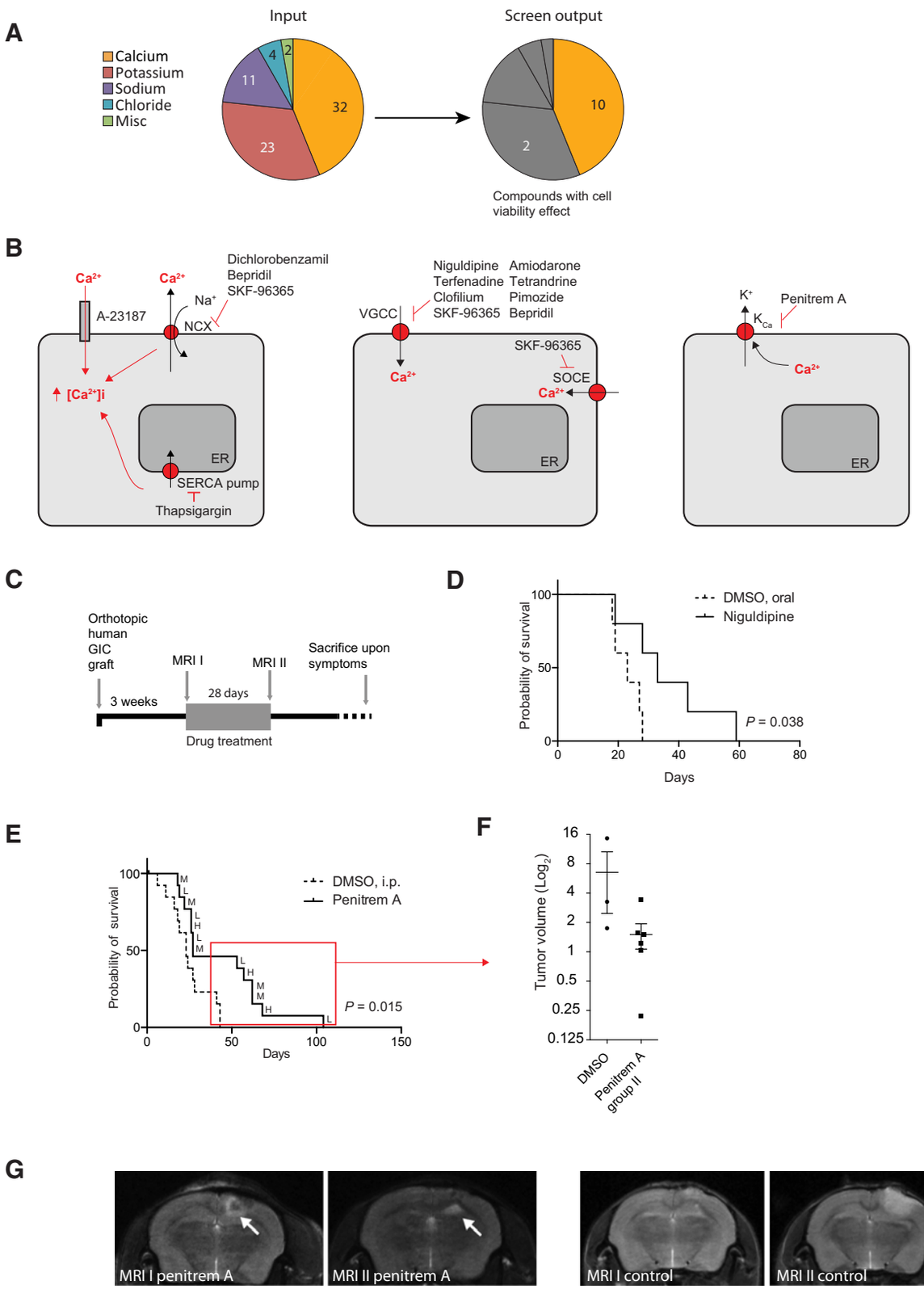

biology approach, we describe the molecular mechanisms of action of these ion channel blockers.

Materials and Methods

For detailed procedures of all methods, see Supplementary Information.

Cell culture

All GIC lines are GBM patient–derived primary cell lines grown as monolayer cultures on laminin in neural stem cell culture media, as described previously (2, 10, 15, 16). Cells were used for experiments between passages 15 and 30, at least one passage after thawing. GliNS1, G179NS, and G166NS were a kind gift from Dr. Peter Dirks (The Hospital for Sick Children, Toronto, Canada) in 2009, at the time of publication (15), and the U3NNN-MG cell lines were obtained continuously from the Uppsala University Human Glioma Cell Culture (HGCC) collection (16). All cells are well characterized (15, 16) and authenticated by short tandem repeat profiling. Cells have been tested negative for mycoplasma using the MycoAlert Plus Mycoplasma Detection Kit (Lonza). Furthermore, RNA sequencing of the GliNS1, G179NS, and G166NS lines verified expression of the markers for glioma subtype as published previously (15).

Drug screening

In the primary screen, Ion Channel Library (Biomol, catalog #2805) as well as clofilium (Sigma-Aldrich) and terfenadine (Sigma-Aldrich) were added (10 μmol/L) to the 384-well microplates 24 hours after GIC seeding, followed by 48-hour incubation, in at least three independent experiments, and analyzed with CellTiterGlo viability assay (Promega). In the secondary screen, 48 GIC lines (U3NNN-MG series) were screened in dose–response in 384 microplates. Subsequent analyses were done in 96-well format using the CellTiterGlo assay.

Xenograft injections

The animal experiments were performed in accordance with the regulations at the Regional Ethical Committee at Haukeland University Hospital. Biopsy spheroid cultures (P3) were prepared as described previously (17) and implanted into the brain parenchyma of NOD/SCID mice (18). Tumor growth was monitored by MRI scanning. Animals received compound or DMSO daily for 28 days. Survival data were plotted according to the Kaplan–Meier method (GraphPad PRISM 6.0d).

Proteomics and phosphoproteomics analyses

Protein expression levels and phosphoproteomics analyses at 0 (control), 2, and 6 hours upon niguldipine treatment (10 μmol/L) were performed using a dimethyl approach (19). For the phosphoproteome analysis, Ti^{4+}-IMAC phosphopeptide enrichment was performed (20) prior to LC/MS-MS analysis.

RNA sequencing

GICs were treated as indicated for 7 hours and subsequent sample preparation, sequencing and analysis was done as described previously (10). Briefly, the Illumina Low-Throughput TruSeq RNA Sample Preparation Kit protocol was used for barcoded cDNA library preparation. Samples were sequenced on an Illumina HiSeq 2000 sequencer.

Immunocytochemistry, IHC, and Western blot analysis

Immunocytochemical staining was done overnight at 4°C using antibodies against DDIT3 (Abcam) and BiP (Abcam). Immunohistochemical analysis on sections from patient samples was performed using antibodies against CACNA1G (HPA004714, The Human Protein Atlas, Sweden) and CACNA1H (HPA39125). Western blot analysis was performed using antibodies against anti-PERK and anti-phospho-EIF2alpha (Cell Signaling Technology). Total protein was detected on the membrane using Coomassie brilliant blue G-250 and analyzed with Image Lab 5.2.1 software (Bio-Rad).

Membrane potential measurement

For membrane potential measurements, GICs were dissociated to a single-cell suspension and preincubated for 30 minutes with DiBAC (1 μmol/L; Invitrogen). After compound addition, cells were incubated for indicated time periods and immediately analyzed by flow cytometry (FACScan; BD Biosciences).

Live-cell Na^+ imaging

For Na^+ imaging, cells (U3013MG) were seeded on laminin-coated coverslips at approximately 70% confluency. The next day, GIC culture medium was exchanged for DMEM without phenol red (Gibco, Life Technologies, 21063-029) and cells were loaded with the Na^+-sensitive dye Asante NaTRIUM Green-2 (5 μmol/L, TEFLabs). Niguldipine (20 μmol/L, Tocris) and penitrem A (20 μmol/L, Tocris) were added directly to the media.

Amino acid uptake assay

GIC line G166NS was selected and 25,000 cells/well were seeded on day 1 onto laminin-coated 24-well, flat-bottom plates

Figure 1.

VGCC and K_{Ca} blockers affect viability of GICs and tumor growth *in vivo*. **A,** A primary screen of 72 ion channel blockers (10 μmol/L) in four GIC lines identified 12 compounds that reduced GIC viability >30% upon 48 hours of compound exposure (threshold set to 0.70 in an ATP-based cell viability assay). The viability was calculated as the ratio between each compound and DMSO control ($n \geq 3$). Pie charts show relative distribution of ion channels targeted by the 12 hit compounds. **B,** Overview of identified compounds and target categories related to Ca^{2+}. SERCA, sarco/endoplasmic reticulum Ca^{2+}-ATPase pump; VGCC, voltage gated Ca^2+ channels; K_{Ca}, Ca^{2+}-gated K^+ channels; NCX, Na^+/Ca^{2+} exchanger; SOCE, store-operated Ca^{2+}-entry. **C,** To assay the effects of ion channel blockers *in vivo*, patient-derived GBM spheroids were implanted stereotactically into mice brains. Three weeks after implantation, tumor growth was confirmed by MRI, and the animals started receiving daily doses of niguldipine (oral) or penitrem A (intraperitoneal injection). Control animals were treated with DMSO. **D,** Kaplan–Meier analysis of niguldipine-treated mice (3.3 mg/kg; $n = 5$) and DMSO-treated control mice ($n = 5$), $P = 0.038$. **E,** Kaplan–Meier analysis of mice treated with penitrem A ($n = 13$) compared with control animals ($n = 13$), $P = 0.015$. Three doses were tested: 1.0 mg/kg (H), 0.33 mg/kg (M), or 0.11 mg/kg (L) as indicated. However, as adverse effects on behavior occurred in some mice after 1–2 days by the H and M doses, all animals were given the L dose for the remaining days of the treatment period. Red box, animals that were alive at the MRI II time point. **F,** In the cohort of responders (red box in E), tumor volume changes measured by MRI I and MRI II were compared with matched controls. **G,** MRI images of sections of the brain hemispheres of the mouse with the longest survival, at MRI time points I and II. Arrows, tumor area. A representative control animal is shown for comparison.

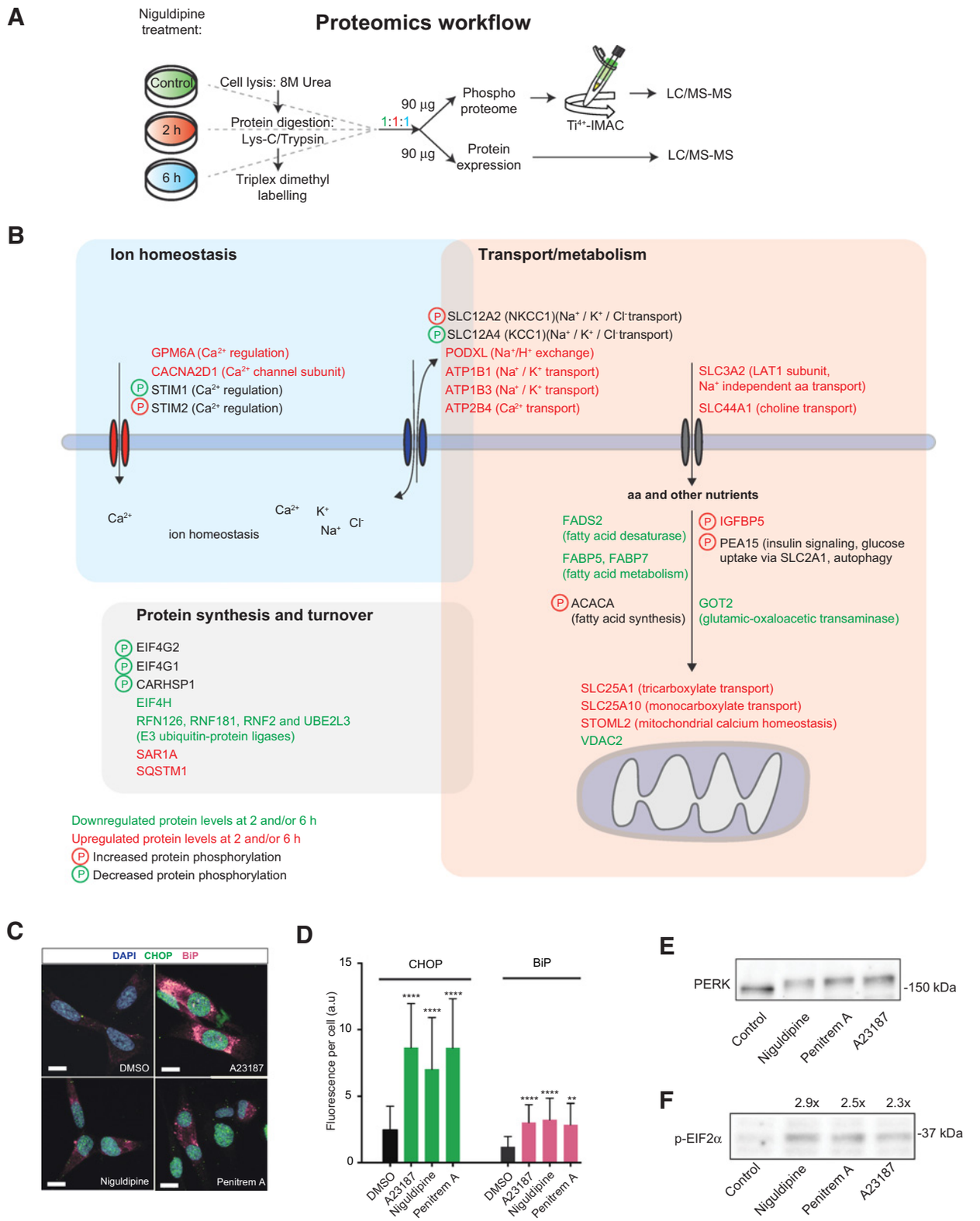

(VWR). L-[14C(U)]-Glutamic Acid (14C-glutamate)(PerkinElmer; 1 μCi) was added to each well and incubated at 37 °C for 30 minutes to allow active uptake. Labeled cells were washed 3 times with ice-cold PBS and dissolved in 150 μL 0.5 mol/L sodium hydroxide. All 150 μL was measured for radioactivity using Aquasafe 300 Plus scintillation cocktail fluid (Zinsser Analytic) and Wallac 1209 Rackbeta liquid scintillation counter (LKB). The radioactive readout of the compound-treated samples was normalized against the DMSO-treated samples.

Results

A screen of ion channel blockers identifies Ca^{2+} channel blockers and targets that decrease GIC viability

To explore the spectrum of channel blockers that might target glioma cell viability, we used patient-derived glioblastoma cells cultured in neural stem cell media on laminin. These cell culture conditions maintain the GICs (15), in contrast to serum-grown GBM cell lines, and we henceforth use the term GIC. We screened a library of 72 ion channel blockers in four different GIC lines (Supplementary Table S1). Of these, 12 induced at least a 30% decrease in cell viability (Fig. 1A and B; Supplementary Table S1). Notably, these drugs act at different points in the Ca^{2+} signaling network, although clofilium and the penitrem A are categorized as K^+ channel blockers (Fig. 1B). As some of the hit compounds also have Ca^{2+}-unrelated targets [such as α-adrenergic receptors and human ether-à-go-go-related gene (hERG) channels] that are expressed in GICs (data not shown), we performed a counter-screen against these targets. No or weak effect on cell viability was observed (Supplementary Fig. S1A and S1B), suggesting that Ca^{2+} homeostasis is the main target for the identified ion channel blockers.

The two most potent compounds identified in the channel blocker screen were the Ca^{2+}-ionophore A23187 and the sarco/endoplasmic reticulum Ca^{2+}-ATPase (SERCA) pump inhibitor thapsigargin (Fig. 1A and B), which we have previously reported to efficiently eradicate GICs (10). Interestingly, eight out of the ten novel compounds identified were VGCC inhibitors, among which niguldipine was the most efficient to reduce cell viability (Supplementary Table S1). The calcium-activated potassium channel (K_{Ca}) blocker penitrem A showed similar efficacy compared with niguldipine. Noteworthy, K_{Ca} channels are K^+-permeable channels that may coassemble with VGCCs in functional nanodomains (21) and become activated in response to elevated intracellular Ca^{2+}, and cooperate to regulate membrane potential (21). VGCCs are assembled by >20 different channel-forming and modulatory subunits (α, $\alpha_2\delta$, β, and γ), and they are overexpressed in cancer cells (Pedersen and Stock, 2013), which provides grounds for cell specificity. Therefore, niguldipine and penitrem A were chosen for further validation.

Niguldipine and penitrem A increase survival in a mouse model of human GBM

Forty-five additional low-passage GIC lines from the HGCC repository (16) were next tested for niguldipine and penitrem A sensitivity in dose–response analyses, and viability effects in GICs were compared with normal nonmalignant cells (human astrocytes and fibroblasts) and HepG2 liver carcinoma cells (Supplementary Fig. S1C and S1D; Supplementary Table S2). All GICs were found to be selectively sensitive to niguldipine and penitrem A compared with the reference cell types (Supplementary Fig. S1C and S1D). We next tested whether this drug sensitivity could be linked to a specific GBM subtype (according to the Verhaak classification; ref. 22) of the HGCC lines. However, no such link was found (Supplementary Fig. S1E). GICs have the potential to form gliospheres *in vitro*, but this ability was abolished by niguldipine and penitrem A treatment (Supplementary Fig. S1F).

To investigate ion channel blocker selectivity and efficacy *in vivo*, effects were analyzed in an orthotopic glioma NOD/SCID mouse model (Fig. 1C). Human GBM spheroids [P3 patient–derived cells expressing markers for a classical, CL, subtype (22); Supplementary Fig. S1G] were transplanted into mouse brains (18, 23), and the mice were treated with niguldipine (orally) or penitrem A (intraperitoneal injection). Niguldipine-treated animals had significantly longer median survival (33 days) compared with control animals (21 days, $P = 0.038$; Fig. 1D). Mice treated with penitrem A also showed a significant increase in survival ($P = 0.015$; Fig. 1E) and a trend for lower tumor volume compared with controls in the mice that survived the longest (Fig. 1F). Notably, the longest survivor showed a reduced tumor volume after treatment with the lowest dose of penitrem A (Fig. 1G). The data show that GBM tumors are sensitive to treatment with VGCCs and K_{Ca} channel blockers *in vivo*.

T-type VGCCs are critical for viability in GIC

As VGCCs are composed of several subfamilies (L-type, T-type, R-type, P/Q type, and N-type), we investigated whether a particular subgroup of VGCCs is targeted by niguldipine and is therefore crucial for GIC survival. The screen and a follow-up dose–response analysis showed that among the dihydropyridines (which block L-type VGCCs), only niguldipine affected significantly GIC viability (Supplementary Fig. S2A). Niguldipine is the only dihydropyridine that has an additional ability to inhibit T-type VGCCs (24); it is reported to inhibit T-type at least 10-fold more efficiently than L-type VGCCs (25), suggesting that T-type VGCCs are crucial for maintaining GIC viability. This was confirmed by the T-type blocker mibefradil, which reduced cell viability at <10 μmol/L concentrations in a dose–response assay in 29 GIC lines (Supplementary Fig. S2B; Supplementary Table S2). In addition, additional blockers towards different VGCCs confirmed the effect by yet another

Figure 2.

VGCC and K_{Ca} block induce the UPR pathway. **A,** Time-course analyses of the proteome and phosphoproteome at 0 (control), 2, and 6 hours in GCs upon niguldipine treatment. Proteins were digested by Lys-C/Trypsin, peptides were labeled using a dimethyl-labeling approach and fractionated by strong cation exchange (SCX) prior to LC/MS-MS for the protein expression levels analysis. For phosphoproteome analysis, Ti^{4+}-IMAC phosphopeptide enrichment was performed prior to LC/MS-MS. **B,** Overview of selected proteins with significantly altered expression or phosphorylation levels ($P \leq 0.05$). **C,** UPR pathway induction in GICs was validated by immunofluorescent staining against CHOP and BiP (encoded by the *HSPA5* gene) at 6 hours after administration of the Ca^{2+} ionophore A23187 (3 μmol/L) or blockers of VGCCs (niguldipine; 5 μmol/L) or K_{Ca} channels (penitrem A; 10 μmol/L). Scale bars, 10 μm. **D,** Statistical analysis of staining in **C** (DMSO control, $n = 46$ cells; A23187, $n = 39$; niguldipine, $n = 24$; penitrem A, $n = 42$; $^{**}P \leq 0.01$; $^{****}P \leq 0.0001$). **E,** Western blot analysis of the ER stress sensor PERK showing an electrophoretic mobility shift upon niguldipine, penitrem A, and A23187 treatment of GICs. **F,** Western blot analysis of phosphorylated EIF2α, the AAR/UPR target, in treated GICs.

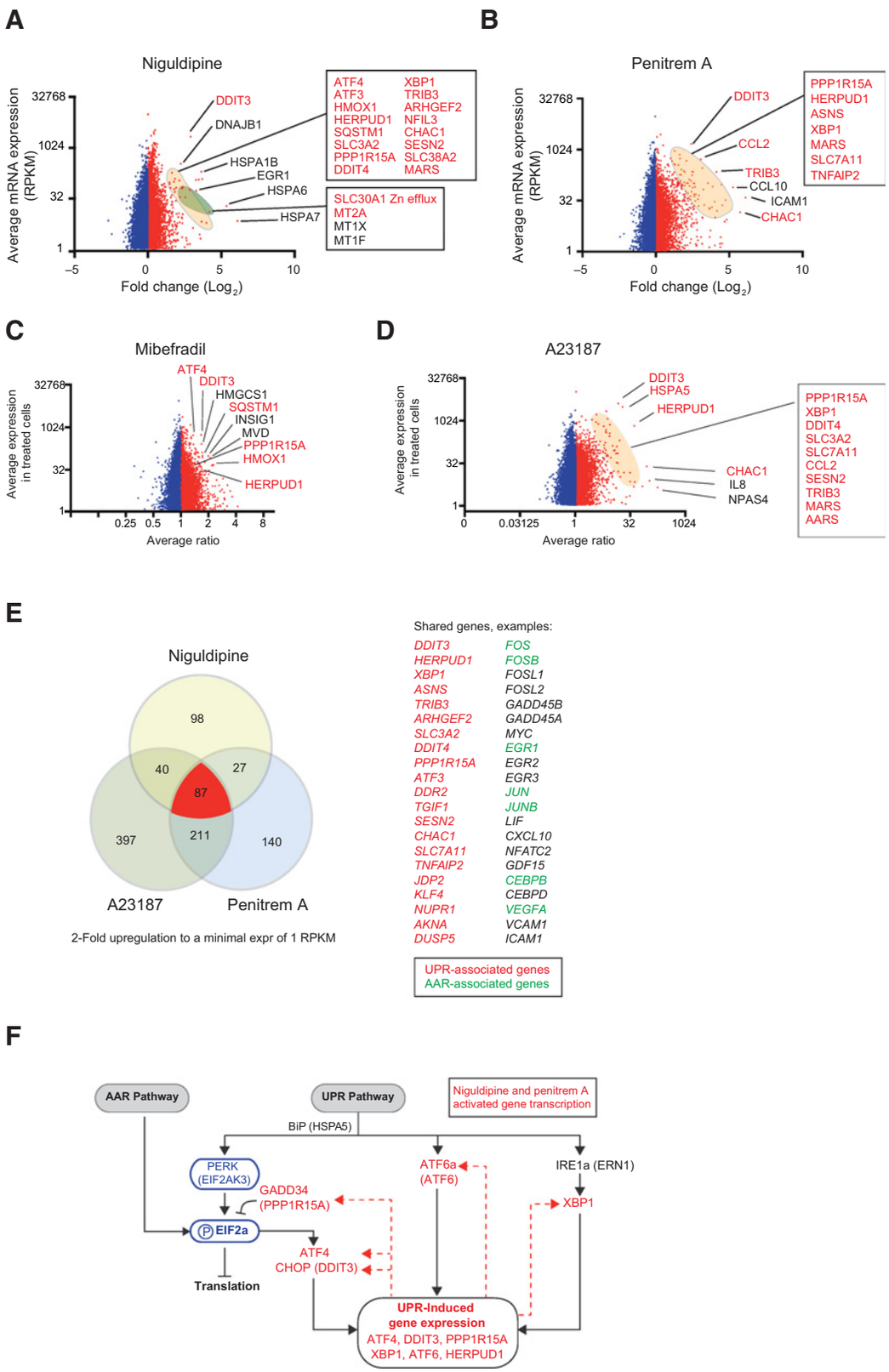

Table 1. List of proteins involved in UPR pathway signaling identified in the (phospho)proteome analysis

	Protein level		Phosphorylation level		
	2 hours	6 hours	2 hours	6 hours	Comments
CCL2	—	2.2	—	—	ATF4 and CHOP target genes
HMOX1	—	2.1	—	—	—
SLC3A2	—	1.7	—	—	—
SQSTM1	—	1.6	—	—	—
HSPA13	—	1.5	—	—	ER chaperones
SEC63	—	1.6	—	—	—
MAN1B1	—	2.1	—	—	ER/Golgi protein involved in glycosylation control
EIF4G2	—	—	—	−3.8	Protein translation
EIF4H	−2.8	—	—	—	—
EEF2	—	—	4.7	8.9	Associated with inhibition of mRNA translation

T-type VGCC blocker (TTA-P2; Supplementary Fig. S2C). Expression of T-type VGCC subunits was also confirmed both on gene and protein level in GIC lines and patient samples, respectively (Supplementary Fig. S2D–S2F). In conclusion, T-type VGCC blockers affected GIC viability and may thus constitute a potential lead targets for eradicating GICs.

Proteomics and phosphoproteomics analysis of channel block in GICs reveals activated unfolded protein response

As the current knowledge of downstream effects elicited by channel blockers is fragmented, we aimed to gain a systems-level understanding of the signaling pathways affected by channel block. To this end, a strategy that included extensive unbiased genome-wide analyses was used. A proteomics and phosphoproteomics approach was employed in a time-course study at 0 (control), 2, and 6 hours upon niguldipine treatment (Fig. 2A; Supplementary Fig. S3A–S3D; Supplementary Table S3) in the GIC line GliNS1. Gene Ontology (GO) analysis of protein expression data showed enrichment for transporters and ion channels, nucleic acid–binding proteins, cytoskeletal proteins, transcription factors, and proteins involved in insulin signaling (Supplementary Fig. S3E; Supplementary Table S4 and S5). The increased expression of proteins involved in ion homeostasis included channels, transporters, and pumps of Ca^{2+}, Na^{+}, K^{+}, and Cl^{-}, such as the ATP1B3 subunit of the Na, K-ATPase that regulates Na^{+} homeostasis (Fig. 2B). This suggests that the cells attempt to restore ion homeostasis. Ion homeostasis may affect nutrient import and, interestingly, the SLC3A2 (a subunit of the amino acid transporter LAT1) was upregulated upon niguldipine treatment (Fig. 2B; Supplementary Table S3). As LAT1 transports several amino acids independently of the plasma membrane Na^{+} gradient, its upregulation may indicate an adaptive response to disturbed ion homeostasis. Aside from LAT1, several other proteins involved in nutrient transport and metabolism were significantly altered upon niguldipine treatment (Fig. 2B). Notably, our data mining of the transcriptome analyses in the report by Hahn and colleagues (26) showed that LAT1 is induced by the unfolded protein response (UPR) pathway, which senses and responds to disturbed ion homeostasis.

In-depth analyses of the proteomics and phosphoproteomics data revealed alterations of a number of proteins associated with the UPR pathway (27, 28) by niguldipine, such as upregulation of target genes of the UPR-associated transcription factors ATF4 and CHOP (Table 1; ref. 26). Other UPR-associated proteins that were found to be altered in response to niguldipine included the following examples: ER chaperones that aid in coping with an excessive unfolded protein load were upregulated, for example, HSPA13, MAN1B1, and SEC63 (a BiP cochaperone; Table 1). Decreased phosphorylation and protein expression levels were found for the translation initiation factors EIF4G2 and EIF4H, respectively, as well as increased phosphorylation levels for the elongation factor EEF2 (Table 1). These alterations are known to lead to UPR-related translational arrest (26, 29–31).

Immunostaining showed a significant increase in CHOP and the ER chaperone BiP after 15-hour exposure to niguldipine or to penitrem A (Fig. 2C and D). These levels were comparable with cells treated with the UPR inducer A23187 (Fig. 2D; ref. 27), confirming UPR activation for both VGCC and K_{Ca} blockers. In addition, the ER stress sensor PERK showed altered electrophoretic mobility for niguldipine, penitrem A, and A23187, probably due to a posttranslational modification, that is, phosphorylation (Fig. 2E; ref. 32). A shared mediator of both UPR and the related amino acid response (AAR; refs. 33, 34) pathway is phosphorylation of EIF2α (p-EIF2α), and Western blot analysis showed robust increase in p-EIF2α (Fig. 2F).

Reactome analysis identifies induction of AAR in addition to UPR

To further explore the downstream signaling activated by VGCC/K_{Ca} block by niguldipine and penitrem A, we employed an orthogonal approach: we investigated changes at the RNA level by analyzing drug-induced transcriptome by RNA sequencing in the GIC line GliNS1 after 7-hour treatment and compared with mibefradil and A23187 (Supplementary Table S6A–S6D). The majority of genes highly induced by niguldipine and penitrem A treatment were UPR-associated (Fig. 3A and B), and were similar to the reactome induced by mibefradil (T-type VGCC blocker; Fig. 3C) and A23187 (which is known to induce

Figure 3.

The UPR-related AAR pathway is induced upon T-type VGCC and K_{Ca} block. **A–D,** Effect of VGCC and K_{Ca} channel block on the UPR-dependent transcriptional response. Plots of RNA sequencing–based gene expression levels versus fold change after 7-hour exposure to niguldipine (10 μmol/L; **A**), penitrem A (10 μmol/L; **B**), mibefradil (10 μmol/L; **C**), and A23187 (10 μmol/L, data from ref. 10; **D**) in GliNS1 GICs. RPKM, reads per kilobase transcript per million reads. **E,** Venn diagram of shared gene expression responses to A23187, niguldipine, and penitrem A. UPR-induced transcripts are shown in red (identified by Han and colleagues, ref. 26) and AAR-associated genes in green. **F,** Overview of the AAR/UPR pathway and its main transcriptional targets (with shared drug induced targets in red).

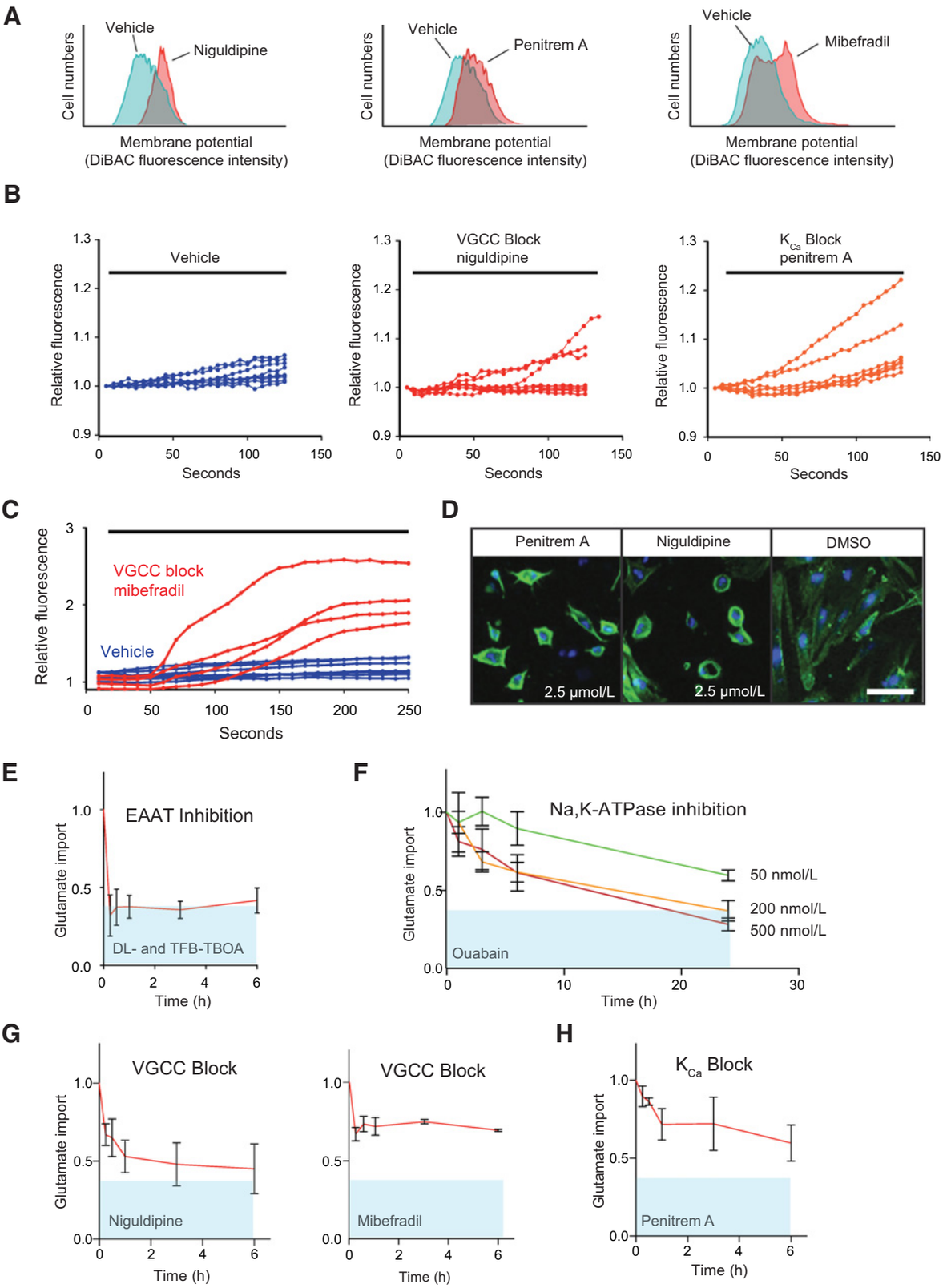

Table 2. AAR-associated genes induced by niguldipine and penitrem A

	Niguldipine	Penitrem A
ASNS	2.4×	8.0×
ATF3	4.0×	4.7×
ATF4	1.7×	2.5×
DDIT3 (CHOP)	7.8×	5.2×
SLC7A1 (CAT-1)	1.2×	2.7×
CEBPB	3.4×	6.0×
FOS	6.9×	5.7×
CALR	1.4×	1.0×
JUNB	2.4×	3.9×
VEGFA	2.4×	4.0×
MYC	2.0×	3.4×

NOTE: Fold change in mRNA expression in treated cells (RNA sequencing RPKM).

UPR; Fig. 3D, data from ref. 10). A Venn analysis of the genes in the drug reactome with at least 2-fold upregulation revealed that 87 upregulated genes were shared by A23187, niguldipine, and penitrem A (Fig. 3E), many of which are UPR-associated. Twenty-one of the 87 identified genes were previously reported to be transcriptional targets of ATF4 or CHOP (26) in the UPR pathway, for example, *DDIT3* and *HERPUD1*. These data suggest induction of the UPR as a primary transcriptional response to VGCC/K_{Ca} block.

We also observed that ATF4/CHOP-independent genes involved in activation of the AAR pathway (33, 34) were induced by VGCC/K_{Ca} block (Fig. 3E; Table 2). The AAR overlaps with the UPR, but is a more restricted and distinct response to amino acid starvation. The finding that the dominant response to VGCC/K_{Ca} channel block was induction of UPR as well as AAR thus suggests that altered ion homeostasis and amino acid starvation are upstream causative events (Fig. 3F).

VGCC and K_{Ca} block leads to membrane depolarization and increased influx of Na^+

Ion channel blockers may affect ion fluxes and, potentially, membrane potential, and our data suggested similar downstream effects for T-type VGCCs and K_{Ca} channels. K_{Ca} channels are known to regulate membrane potential, and the block of these channels is expected to result in depolarization. We therefore analyzed the effects on membrane potential by niguldipine, penitrem A, and mibefradil, using the membrane potential–sensitive fluorescent dye DiBAC and flow cytometry. This confirmed that the three ion channel blockers induced depolarization in GICs in a similar manner within 15 minutes of treatment (Fig. 4A), indicating a converging mechanism. Changes in membrane potential may in turn affect many voltage-gated channels such as Na^+-permeable channels. To investigate this possibility, a Na^+-sensitive dye (Asante NaTRIUM green-2) was used to monitor changes in intracellular Na^+ levels during treatment. This showed that niguldipine and penitrem A induced a surge of intracellular Na^+ within minutes (Fig. 4B) and a similar effect was also found for mibefradil (Fig. 4C). Thus, blocking either T-type VGCC or K_{Ca} channels seemed to alter ion homeostasis in a similar manner, which is critical for cell survival in GICs. This is further supported by the fact that the two channels may associate into a functional electrophysiological unit (21).

T-type VGCC and K_{Ca} block leads to cell shrinkage prior to cell death

Analysis of cell-cycle progression and cell death upon niguldipine treatment (40 hours; 10 μmol/L) showed a moderate induction of apoptosis (Supplementary Fig. S4A), an increase in sub-2n cellular debris (Supplementary Fig. S4B), which may be a consequence of apoptosis or necrosis (Supplementary Fig. S4C). This suggests that cell-cycle arrest and cell death occurred simultaneously. Live imaging also revealed an apparent change in morphology of GICs within 2 to 6 hours of administration of either niguldipine or penitrem A, in which the cells shrunk and rounded up (Supplementary Fig. S4D). Administration of sublethal doses of niguldipine and penitrem A demonstrated that this change in morphology was sustained after washout of blocker (Fig. 4D).

T-type VGCC and K_{Ca} block cause loss of Na^+-dependent nutrient transport

We hypothesized that the cell shrinkage observed might be due to nutrient starvation caused by disturbance of the Na^+ gradient, which drives nutrient transport via an extensive set of Na^+-dependent transporters. To test this hypothesis, we analyzed uptake of a radiolabeled glutamate over time in GICs. GICs import measurable quantities of glutamate via the excitatory amino acid transporter (EAAT) family of transporters and may be used to determine general Na^+-dependent transport. First, we determined the level of Na^+-dependent versus Na^+-independent transport using inhibition of the EAAT transporters, which showed that approximately 60% of the glutamate transport was Na^+-dependent (Na^+-independent transport indicated as blue area; Fig. 4E). A similar reduction in glutamate transport was seen by inhibition of the Na, K-ATPase, which is critical in establishing the Na^+ gradient (Fig. 4F). Notably, inhibition of the Na, K-ATPase was recently shown to cause induction of the UPR/AAR pathways (35) similar to our results on T-type VGCC and K_{Ca} channel block. Further supporting a shared mechanism, niguldipine, mibefradil, and penitrem A caused glutamate transport decrease within 15 minutes of exposure to drug and the effect was sustained (6 hours; Fig. 4G and H). The data showed that

Figure 4.

T-type VGCC and K_{Ca} block affects membrane potential and ion homeostasis and leads to loss of Na^+-dependent nutrient transport. **A,** To analyze the immediate effects on ion homeostasis by selected compounds, membrane potential was analyzed by flow cytometry (10,000 cells) after loading GICs with DiBAC reporter dye, followed by drug exposure for 15 minutes of 20 μmol/L niguldipine, 20 μmol/L penitrem A, or 20 μmol/L mibefradil. Histograms show one representative experiment ($n = 3$). **B,** Live imaging of intracellular Na^+ levels in GICs was performed after loading of the Na^+-indicator dye Asante NaTRIUM green-2 and treatment with vehicle control (DMSO) or niguldipine (20 μmol/L) or penitrem A (30 μmol/L). **C,** Extended live imaging of intracellular Na^+ levels in GICs after treatment with vehicle control and mibefradil (20 μmol/L). **D,** GIC cells (GliNS1) were imaged after 48 hours of sublethal doses (2.5 μmol/L) of niguldipine or penitrem A, followed by a 48-hour wash-out. Staining of cytoskeleton (phalloidin-488; green) and nuclei (TO-PRO-647; blue). **E–H,** Time-course uptake assay of radiolabeled glutamate in GICs upon ion blocker treatment. The import is reported as ratio treated/control ($n = 3$). **E,** Inhibitors of Na^+-dependent amino acid transporters of the EAAT family (18 μmol/L DL-TBOA + 66 nmol/L TFB-TBOA). **F,** Ouabain (50–500 nmol/L), which inhibits the sodium pump Na, K-ATPase. **G,** T-type VGCC blockers niguldipine or mibefradil (10 μmol/L). **H,** K_{Ca} blocker penitrem A (10 μmol/L). The areas in light blue indicate residual Na^+-independent uptake of radiolabeled glutamate.

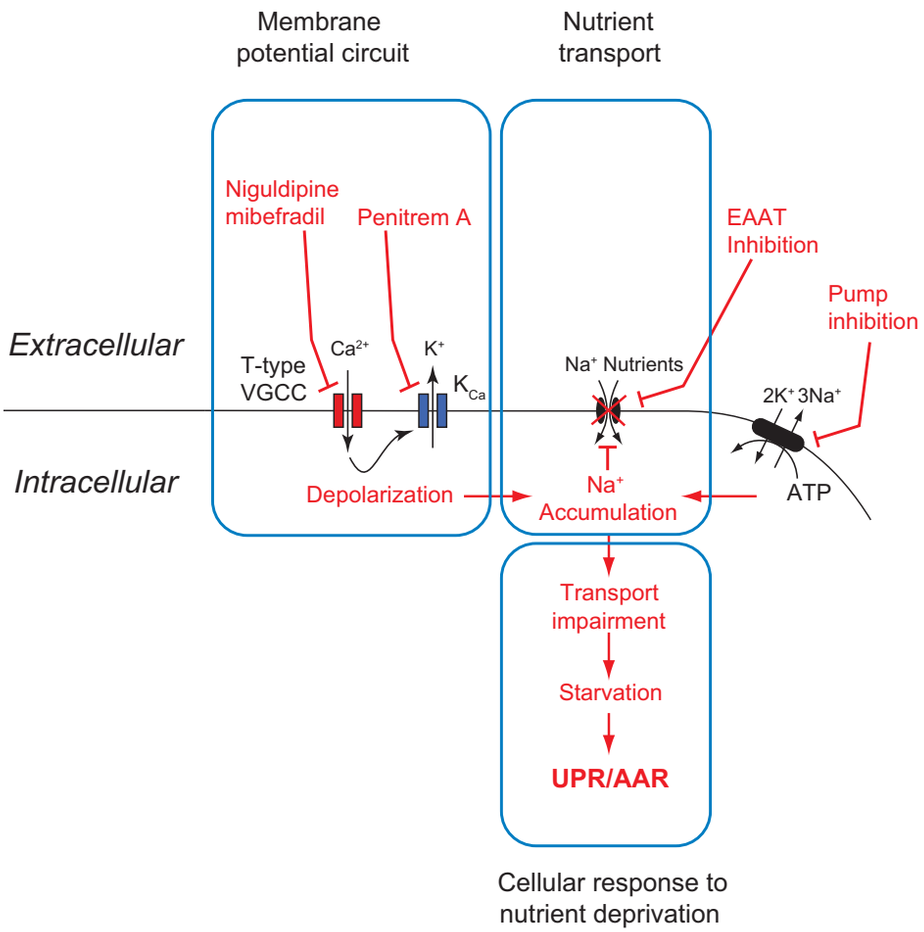

Figure 5.
Model of mechanisms and pathways affected by VGCC and K_{Ca} block. T-type VGCCs and K_{Ca} channels may act together to control membrane potential. Blockers cause membrane depolarization, followed by disturbed ion homeostasis including increase in intracellular $[Na^+]$. The surge of $[Na^+]_i$ blocks the Na^+-dependent transport of nutrients and ultimately leads to starvation. The effect can be phenocopied by selective block of Na^+-dependent glutamate transport as well as by block of the Na, K-ATPase, which causes dissipation of the Na^+ gradient. A residual import of glutamate may be accounted for by Na^+-independent transport.

Na^+-dependent transport was abrogated by niguldipine and penitrem A, unlike the residual Na^+-independent uptake (blue area in Fig. 4E–H). In summary, the results show that Ca^{2+} signaling blockers, such as niguldipine and penitrem A, cause membrane depolarization, increase in intracellular Na^+ in GICs, which in turn leads to decreased Na^+-dependent transport and ultimately to nutrient starvation. This sequence of events explains the subsequent induction of UPR/AAR pathways (Fig. 5).

Discussion

Previous reports have shown the involvement of catabolic cellular pathway using blockers against VGCCs in cancer cells (12, 13). However, to date, the knowledge regarding pathways activated downstream of such ion channel blockers have remained limited and fragmented. For the first time, using a multi-angle approach, we comprehensively describe how both T-type VGCC and K_{Ca} ion channel blockers initiate downstream effects compromising tumor cell viability. GICs responded to block of these channels in a similar manner; block leads to reduction in Na^+-dependent nutrient transport and induction of the UPR and AAR pathways. Interestingly, the K_{Ca} channel blocker paxilline was previously identified to enhance apoptosis in serum-cultured glioma cells via a CHOP-mediated pathway (36). Moreover, activation of the vanilloid receptor TRPV1 promotes cell death in astrocytomas via ATF3 (14), which is upregulated in the UPR and AAR pathways (26). These reports thus support our data showing that ion channel–mediated cell death occurs via an extensive induction of UPR and AAR. In addition, data mining the report by Han and colleagues (26) and our data show that the ATF4- and CHOP-mediated transcriptome responses involve increased expression of a number of amino acid transporters that are Na^+-independent. Our finding that transport deficiency precedes UPR/AAR activation suggests a core capacity of the UPR/AAR pathways to respond to and possibly counteract the nutrient shortage caused by dissipated Na^+ gradient. Notably, as the Na^+ gradient is essential to drive import/export of numerous nutrients and ions, we suggest that the effect by channel blockers on nutrient import may be extensive. Investigations to determine the contribution of individual members of the large family of Na^+-dependent transporters toward UPR/AAR induction and cell death will be important to understand cellular response to nutrient starvation. Such studies will also shed light on potential similarities between stem cells and cancer stem cells regarding metabolism.

T-type VGCC and K_{Ca} channels have previously attracted attention as targets in glioma cell lines (25, 37–47). Our study extends the importance of T-type VGCCs and K_{Ca} channels as appealing targets in tumor-initiating cells. Importantly, for the first time, we show that niguldipine and penitrem A target selectively GIC growth and not normal cell growth *in vitro* and *in vivo*. This suggests that cancer cells are more sensitive to ion disturbance

compared with other cell types. Interestingly, niguldipine has been shown to reduce resistance to the chemotherapeutic agent mitoxantrone in breast cancer cells, via inhibition of the ABC transporter ABCG2 (48). ABCG2 is overexpressed in brain tumor stem cells compared with normal cancer cells and underlies resistance to chemotherapeutic agents by drugs efflux (49). As chemoresistance in GICs may result in tumor recurrence, it is essential to develop drug strategies that target this cell population. Our *in vivo* data show increased survival in a mouse model for human GBM upon niguldipine and penitrem A treatment. Therefore, studies involving, for example, niguldipine as adjuvant or additive to the standard chemotherapy for patients affected by GBM would warrant consideration.

In conclusion, our mechanistic findings show that targeting essential cancer cell metabolism via depolarizing drugs is an option for efficient targeting of the resistant GICs. These findings pave the way for further studies of other compounds targeting additional points in the multifaceted network of proteins maintaining membrane potential and nutrient transport.

Disclosure of Potential Conflicts of Interest

No potential conflicts of interest were disclosed.

Authors' Contributions

Conception and design: M. Niklasson, G. Maddalo, B.B. Carson, P. Uhlén, S. Nelander, M. Andäng

Development of methodology: M. Niklasson, G. Maddalo, S. Wee, L.G.J. Hammarström, S. Nelander, M. Andäng

Acquisition of data (provided animals, acquired and managed patients, provided facilities, etc.): M. Niklasson, G. Maddalo, E. Mutlu, S. Wee, P. Sekyrova, N. Fritz, I. Dehnisch, G. Kyriatzis, M. Krafcikova, B.B. Carson, J. Feenstra, A.F.M. Altelaar, S. Linnarsson, P. Uhlén, P.Ø. Enger

Analysis and interpretation of data (e.g., statistical analysis, biostatistics, computational analysis): M. Niklasson, G. Maddalo, Z. Sramkova, E. Mutlu, S. Wee, N. Fritz, I. Dehnisch, G. Kyriatzis, M. Krafcikova, B.B. Carson, J. Feenstra, V.D. Marinescu, M. Haraldsson, A.-L. Gustavsson, L.G.J. Hammarström, A. Jenmalm-Jensen, A.F.M. Altelaar, P. Uhlén, P. Uhlén, L. Trantirek, C.T. Vincent, S. Nelander, M. Andäng

Writing, review, and/or revision of the manuscript: M. Niklasson, G. Maddalo, E. Mutlu, S. Wee, P. Sekyrova, N. Fritz, G. Kyriatzis, B.B. Carson, A. Segerman, C.T. Vincent, S. Nelander, P.Ø. Enger, M. Andäng

Administrative, technical, or material support (i.e., reporting or organizing data, constructing databases): M. Niklasson, G. Maddalo, E. Mutlu, S. Wee, G. Kyriatzis, L. Uhrbom, P.Ø. Enger

Study supervision: P. Uhlén, S. Nelander, P.Ø. Enger, M. Andäng

Acknowledgments

We thank Victor N. Ubele (Merck) for TTA-P2 compound, Peter B. Dirks (The Hospital for Sick Children/University of Toronto, Toronto, Canada) for providing GIC lines, Annika Hermansson (IGP, Uppsala University, Uppsala, Sweden) for help with immunohistochemistry, and Jan Mulder (Science for Life Laboratory) for providing antibodies.

Grant Support

M. Niklasson, P. Sekyrova, and G. Maddalo were awarded postdoctoral fellowships from the Swedish Childhood Cancer Foundation, the Swedish Cancer Foundation, and the Swedish Research Council, respectively. The study was supported by grants to M. Andäng from Swedish Research Council, Swedish Cancer Foundation, Swedish Childhood Cancer Foundation, Karolinska Institutet, Grant Agency of the Czech Republic (GA15-20818S), CEITEC 2020 (LQ1601) project with financial contribution made by the Ministry of Education, Youths and Sports of the Czech Republic within special support paid from the National Programme for Sustainability II funds. The study was also supported by grants to T. Vincent from the Swedish Cancer Foundation and to A.F.M Altelaar by the Netherlands Organization for Scientific Research (NWO) as part of the National Roadmap Large-Scale Research Facilities of the Netherlands (project number 184.032.201), the Prime XS-Consortium, seventh framework EU (XS-000158).

The costs of publication of this article were defrayed in part by the payment of page charges. This article must therefore be hereby marked *advertisement* in accordance with 18 U.S.C. Section 1734 solely to indicate this fact.

Received August 23, 2016; revised November 9, 2016; accepted November 29, 2016; published OnlineFirst January 13, 2017.

References

1. Galli R, Binda E, Orfanelli U, Cipelletti B, Gritti A, De Vitis S, et al. Isolation and characterization of tumorigenic, stem-like neural precursors from human glioblastoma. Cancer Res 2004;64:7011–21.
2. Singh SK, Hawkins C, Clarke ID, Squire JA, Bayani J, Hide T, et al. Identification of human brain tumour initiating cells. Nature 2004;432:396–401.
3. Ben-Porath I, Thomson MW, Carey VJ, Ge R, Bell GW, Regev A, et al. An embryonic stem cell-like gene expression signature in poorly differentiated aggressive human tumors. Nat Genet 2008;40:499–507.
4. Holmberg J, He X, Peredo I, Orrego A, Hesselager G, Ericsson C, et al. Activation of neural and pluripotent stem cell signatures correlates with increased malignancy in human glioma. PLoS One 2011;6:e18454.
5. Lathia JD, Mack SC, Mulkearns-Hubert EE, Valentim CL, Rich JN. Cancer stem cells in glioblastoma. Genes Dev 2015;29:1203–17.
6. Bao S, Wu Q, McLendon RE, Hao Y, Shi Q, Hjelmeland AB, et al. Glioma stem cells promote radioresistance by preferential activation of the DNA damage response. Nature 2006;444:756–60.
7. Liu G, Yuan X, Zeng Z, Tunici P, Ng H, Abdulkadir IR, et al. Analysis of gene expression and chemoresistance of CD133+ cancer stem cells in glioblastoma. Mol Cancer 2006;5:67.
8. Schickling BM, Aykin-Burns N, Leslie KK, Spitz DR, Korovkina VP. An inhibitor of K+ channels modulates human endometrial tumor-initiating cells. Cancer Cell Int 2011;11:25.
9. Liu M, Inoue K, Leng T, Guo S, Xiong ZG. TRPM7 channels regulate glioma stem cell through STAT3 and Notch signaling pathways. Cell Signal 2014;26:2773–81.
10. Wee S, Niklasson M, Marinescu VD, Segerman A, Schmidt L, Hermansson A, et al. Selective calcium sensitivity in immature glioma cancer stem cells. PLoS One 2014;9:e115698.
11. Pedersen SF, Stock C. Ion channels and transporters in cancer: pathophysiology, regulation, and clinical potential. Cancer Res 2013;73:1658–61.
12. Kania E, Pajak B, Orzechowski A. Calcium homeostasis and ER stress in control of autophagy in cancer cells. Biomed Res Int 2015;2015:352794.
13. Zhang L, Yu J, Pan H, Hu P, Hao Y, Cai W, et al. Small molecule regulators of autophagy identified by an image-based high-throughput screen. Proc Natl Acad Sci U S A 2007;104:19023–8.
14. Stock K, Kumar J, Synowitz M, Petrosino S, Imperatore R, Smith ES, et al. Neural precursor cells induce cell death of high-grade astrocytomas through stimulation of TRPV1. Nat Med 2012;18:1232–8.
15. Pollard SM, Yoshikawa K, Clarke ID, Danovi D, Stricker S, Russell R, et al. Glioma stem cell lines expanded in adherent culture have tumor-specific phenotypes and are suitable for chemical and genetic screens. Cell Stem Cell 2009;4:568–80.
16. Xie Y, Bergstrom T, Jiang Y, Johansson P, Marinescu VD, Lindberg N, et al. The human glioblastoma cell culture resource: validated cell models representing all molecular subtypes. EBioMedicine 2015;2:1351–63.
17. Bjerkvig R, Tonnesen A, Laerum OD, Backlund EO. Multicellular tumor spheroids from human gliomas maintained in organ culture. J Neurosurg 1990;72:463–75.
18. Wang J, Miletic H, Sakariassen PO, Huszthy PC, Jacobsen H, Brekka N, et al. A reproducible brain tumour model established from human glioblastoma biopsies. BMC Cancer 2009;9:465.

19. Boersema PJ, Raijmakers R, Lemeer S, Mohammed S, Heck AJ. Multiplex peptide stable isotope dimethyl labeling for quantitative proteomics. Nat Protoc 2009;4:484–94.
20. Zhou H, Ye M, Dong J, Corradini E, Cristobal A, Heck AJ, et al. Robust phosphoproteome enrichment using monodisperse microsphere-based immobilized titanium (IV) ion affinity chromatography. Nat Protoc 2013; 8:461–80.
21. Fakler B, Adelman JP. Control of K(Ca) channels by calcium nano/microdomains. Neuron 2008;59:873–81.
22. Verhaak RG, Hoadley KA, Purdom E, Wang V, Qi Y, Wilkerson MD, et al. Integrated genomic analysis identifies clinically relevant subtypes of glioblastoma characterized by abnormalities in PDGFRA, IDH1, EGFR, and NF1. Cancer Cell 2010;17:98–110.
23. Sundlisaeter E, Wang J, Sakariassen PO, Marie M, Mathisen JR, Karlsen BO, et al. Primary glioma spheroids maintain tumourogenicity and essential phenotypic traits after cryopreservation. Neuropathol Appl Neurobiol 2006;32:419–27.
24. Romanin C, Seydl K, Glossmann H, Schindler H. The dihydropyridine niguldipine inhibits T-type Ca2+ currents in atrial myocytes. Pflugers Arch 1992;420:410–2.
25. Stengel W, Jainz M, Andreas K. Different potencies of dihydropyridine derivatives in blocking T-type but not L-type Ca2+ channels in neuroblastoma-glioma hybrid cells. Eur J Pharmacol 1998;342:339–45.
26. Han J, Back SH, Hur J, Lin YH, Gildersleeve R, Shan J, et al. ER-stress-induced transcriptional regulation increases protein synthesis leading to cell death. Nat Cell Biol 2013;15:481–90.
27. Park HR, Tomida A, Sato S, Tsukumo Y, Yun J, Yamori T, et al. Effect on tumor cells of blocking survival response to glucose deprivation. J Natl Cancer Inst 2004;96:1300–10.
28. Drummond IA, Lee AS, Resendez EJr., Steinhardt RA. Depletion of intracellular calcium stores by calcium ionophore A23187 induces the genes for glucose-regulated proteins in hamster fibroblasts. J Biol Chem 1987;262: 12801–5.
29. Wang M, Wey S, Zhang Y, Ye R, Lee AS. Role of the unfolded protein response regulator GRP78/BiP in development, cancer, and neurological disorders. Antioxid Redox Signal 2009;11:2307–16.
30. Andruska ND, Zheng X, Yang X, Mao C, Cherian MM, Mahapatra L, et al. Estrogen receptor alpha inhibitor activates the unfolded protein response, blocks protein synthesis, and induces tumor regression. Proc Natl Acad Sci U S A 2015;112:4737–42.
31. Browne GJ, Proud CG. A novel mTOR-regulated phosphorylation site in elongation factor 2 kinase modulates the activity of the kinase and its binding to calmodulin. Mol Cell Biol 2004;24:2986–97.
32. Harding HP, Zhang Y, Zeng H, Novoa I, Lu PD, Calfon M, et al. An integrated stress response regulates amino acid metabolism and resistance to oxidative stress. Mol Cell 2003;11:619–33.
33. Shan J, Balasubramanian MN, Donelan W, Fu L, Hayner J, Lopez MC, et al. A mitogen-activated protein kinase/extracellular signal-regulated kinase kinase (MEK)-dependent transcriptional program controls activation of the early growth response 1 (EGR1) gene during amino acid limitation. J Biol Chem 2014;289:24665–79.
34. Kilberg MS, Balasubramanian M, Fu L, Shan J. The transcription factor network associated with the amino acid response in mammalian cells. Adv Nutr 2012;3:295–306.
35. Wei C, Lin M, Jinjun B, Su F, Dan C, Yan C, et al. Involvement of general control nonderepressible kinase 2 in cancer cell apoptosis by posttranslational mechanisms. Mol Biol Cell 2015;26: 1044–57.
36. Kang YJ, Kim IY, Kim EH, Yoon MJ, Kim SU, Kwon TK, et al. Paxilline enhances TRAIL-mediated apoptosis of glioma cells via modulation of c-FLIP, survivin and DR5. Exp Mol Med 2011;43:24–34.
37. Goglia AG, Delsite R, Luz AN, Shahbazian D, Salem AF, Sundaram RK, et al. Identification of novel radiosensitizers in a high-throughput, cell-based screen for DSB repair inhibitors. Mol Cancer Ther 2015;14: 326–42.
38. Valerie NC, Dziegielewska B, Hosing AS, Augustin E, Gray LS, Brautigan DL, et al. Inhibition of T-type calcium channels disrupts Akt signaling and promotes apoptosis in glioblastoma cells. Biochem Pharmacol 2013;85: 888–97.
39. Zhang Y, Wang H, Qian Z, Feng B, Zhao X, Jiang X, et al. Low-voltage-activated T-type Ca2+ channel inhibitors as new tools in the treatment of glioblastoma: the role of endostatin. Pflugers Arch 2014;466: 811–8.
40. Zhang Y, Zhang J, Jiang D, Zhang D, Qian Z, Liu C, et al. Inhibition of T-type Ca(2)(+) channels by endostatin attenuates human glioblastoma cell proliferation and migration. Br J Pharmacol 2012;166: 1247–60.
41. Stegen B, Butz L, Klumpp L, Zips D, Dittmann K, Ruth P, et al. Ca2+-Activated IK K+ channel blockade radiosensitizes glioblastoma cells. Mol Cancer Res 2015;13:1283–95.
42. Keir ST, Friedman HS, Reardon DA, Bigner DD, Gray LA. Mibefradil, a novel therapy for glioblastoma multiforme: cell cycle synchronization and interlaced therapy in a murine model. J Neurooncol 2013;111: 97–102.
43. Panner A, Cribbs LL, Zainelli GM, Origitano TC, Singh S, Wurster RD. Variation of T-type calcium channel protein expression affects cell division of cultured tumor cells. Cell Calcium 2005;37:105–19.
44. Sheehan JP, Xu Z, Popp B, Kowalski L, Schlesinger D. Inhibition of glioblastoma and enhancement of survival via the use of mibefradil in conjunction with radiosurgery. J Neurosurg 2013;118:830–7.
45. Latour I, Louw DF, Beedle AM, Hamid J, Sutherland GR, Zamponi GW. Expression of T-type calcium channel splice variants in human glioma. Glia 2004;48:112–9.
46. Weaver AK, Liu X, Sontheimer H. Role for calcium-activated potassium channels (BK) in growth control of human malignant glioma cells. J Neurosci Res 2004;78:224–34.
47. Basrai D, Kraft R, Bollensdorff C, Liebmann L, Benndorf K, Patt S. BK channel blockers inhibit potassium-induced proliferation of human astrocytoma cells. Neuroreport 2002;13:403–7.
48. Zhou XF, Yang X, Wang Q, Coburn RA, Morris ME. Effects of dihydropyridines and pyridines on multidrug resistance mediated by breast cancer resistance protein: in vitro and in vivo studies. Drug Metab Dispos 2005;33:1220–8.
49. Martin V, Sanchez-Sanchez AM, Herrera F, Gomez-Manzano C, Fueyo J, Alvarez-Vega MA, et al. Melatonin-induced methylation of the ABCG2/BCRP promoter as a novel mechanism to overcome multidrug resistance in brain tumour stem cells. Br J Cancer 2013;108:2005–12.